Calculation of stellar electron-capture cross sections on nuclei based on microscopic Skyrme functionals

Paar, Nils; Colo, G.; Khan, E.; Vretenar, Dario

Calculation of stellar electron-capture cross sections on nuclei based on microscopic Skyrme functionals

N. Paar
Physics Department, Faculty of Science, University of Zagreb, Croatia

G. Colò
Dipartimento di Fisica dell'Università degli Studi and INFN, Sezione di Milano, via Celoria 16, I-20133 Milano, Italy

E. Khan and D. Vretenar
Institut de Physique Nucléaire, IN2P3-CNRS/Université Paris-Sud, F-91406 Orsay, France
(Received 24 July 2009; published 11 November 2009)

A fully self-consistent microscopic framework for the evaluation of nuclear weak-interaction rates at finite temperature is introduced, based on Skyrme functionals. The single-nucleon basis and the corresponding thermal occupation factors of the initial nuclear state are determined in the finite-temperature Skyrme Hartree-Fock model and charge-exchange transitions to excited states are computed using the finite-temperature random-phase approximation (RPA). Effective interactions are implemented self-consistently: Both the finite-temperature single-nucleon Hartree-Fock equations and the matrix equations of RPA are based on the same Skyrme energy density functional. Using a representative set of Skyrme functionals, the model is applied in the calculation of stellar electron-capture cross sections for selected nuclei in the iron mass group and for neutron-rich Ge isotopes.

DOI: 10.1103/PhysRevC.80.055801 PACS number(s): 21.60.Jz, 23.40.Bw, 23.40.Hc, 26.50.+x

I. INTRODUCTION

Nuclear weak-interaction processes play a crucial role in the late stages of the evolution of a massive star and in presupernova stellar collapse [1–3]. The core of a massive star at the end of hydrostatic burning is stabilized by electron degeneracy pressure as long as its mass does not exceed the Chandrasekhar limit of about 1.44 solar masses. If this mass limit is exceeded, electron pressure can no longer stabilize the core, and it collapses. The dynamics of this process depends on the core entropy and lepton-to-baryon ratio Y_e [4], which are essentially determined by weak-interaction processes: nuclear β decay,

$$(Z, N) \longrightarrow (Z+1, N-1) + e^- + \bar{\nu}_e, \tag{1}$$

and electron capture,

$$e^- + (Z, N) \longrightarrow \nu_e + (Z-1, N+1). \tag{2}$$

The latter reduces the number of electrons available for pressure support, whereas β decay acts in the opposite direction. At low matter densities $\rho \leqslant 10^{11}$ g cm^{-3} neutrinos escape from the star, carrying away energy (i.e., cooling the stellar core) and keeping its entropy low. For initial Y_e values of ≈ 0.5, β decays are impeded by the presence of electrons, which reduce the available phase space for decay but become competitive when the composition of nuclei in the core becomes more neutron rich. In the early stage of the collapse, for densities lower than a few 10^{10} g cm^{-3}, the electron chemical potential is of the same order of magnitude as the nuclear Q value and the electron-capture cross sections are sensitive to the details of the Gamow-Teller GT$^+$ strength distributions in daughter nuclei. At these densities and temperatures between 300 and 800 keV, electrons are captured on nuclei with mass number $A \leqslant 60$. For higher densities and temperatures $T \approx 1$ MeV, electron capture occurs on heavier nuclei $A > 65$. Under these conditions, however, the electron chemical potential is significantly higher than the nuclear Q value and the capture rates are determined dominantly by the centroid and the total GT$^+$ strength [2,3].

The first standard tabulation of nuclear weak-interaction rates for astrophysical applications was that of Fuller, Fowler, and Newman [5]. It was based on the independent-particle model but used experimental information whenever available. The tables included rates for electron capture, positron capture, β decay, and positron emission for relevant nuclei in the mass range $21 \leqslant A \leqslant 60$. Based on data on GT$^+$ strength distributions that in the meantime became available and by using large-scale shell-model diagonalization in the complete pf shell, these rates have been improved, and rates for electron and positron captures and for β^+ and β^- decays have been computed for stellar conditions and for more than 100 nuclei in the mass range $A = 45$–65 [6,7]. Using the improved weak-interaction rates, models for presupernova evolution of massive stars were examined in Ref. [8], and it was concluded that the resulting changes in the initial value of Y_e and iron core mass could have important consequences for nucleosynthesis and the supernova explosion mechanism. Detailed calculations of stellar weak-interaction rates in the iron mass region have also been carried out with the shell-model Monte Carlo (SMMC) approach [9]. The advantage of this approach is that it treats nuclear temperature exactly and can even include larger model spaces. There are limitations, however, in applying the SMMC to odd-A and odd-odd nuclei at low temperatures. In addition, the SMMC approach yields only an averaged GT strength distribution, whereas the diagonalization shell-model approach allows for detailed spectroscopy.

At higher densities and core temperatures $T \approx 1$ MeV, the excitation energy of a nucleus with mass number $A \approx 80$ is much larger than the energy gap between the pf and the sdg shells. Weak-interaction rates for nuclei beyond

the pf shell cannot yet be systematically evaluated with large-scale diagonalization shell-model calculations because of huge configuration spaces and the lack of a reliable effective interaction in this mass region. Thus, in Ref. [10] a hybrid model has been introduced in which the nucleus is described as a Slater determinant with temperature-dependent occupation numbers, determined with SMMC calculations. In the second step, the electron-capture rates are computed from GT^+ strength distributions calculated with the random-phase approximation (RPA) built on top of the temperature-dependent Slater determinant. The SMMC/RPA hybrid model was used to calculate electron-capture rates on nuclei with mass numbers $A = 65$–112 at temperatures and densities characteristic for core collapse [11]. It was shown that these rates are so great that electron capture on nuclei dominates over capture on free protons, and this leads to significant changes in the hydrodynamics of core collapse and bounce [11,12].

The latest theoretical and computational advances in modeling the nuclear physics input for astrophysical applications have highlighted the need for fully microscopic global predictions for the nuclear ingredients. This is especially important when considering neutron-rich nuclei far from the line of β stability, for which data on ground-state properties and excitations are not available. The basic advantages of the shell model are the ability to describe simultaneously all spectroscopic properties of low-lying states for a large domain of nuclei and the use of effective interactions that can be related to two- and three-nucleon bare forces. However, because effective interactions depend strongly on the choice of active shells and truncation schemes, there is no universal shell-model interaction that can be used for all nuclei. Moreover, because single-particle energies and a large number of two-body matrix elements have to be adjusted to data, extrapolations to nuclei far from stability are not expected to be very reliable. Medium-heavy and heavy nuclei with very large valence spaces require calculations with matrix dimensions that are far beyond the limits of current shell-model variants. Properties of heavy nuclei with large numbers of active valence nucleons are therefore best described within the framework of nuclear energy density functionals (NEDFs). At present, NEDFs provide the most complete description of ground-state properties and collective excitations over the whole nuclide chart [13,14]. At the level of practical applications the NEDF framework is realized in terms of self-consistent mean-field models. With a small set of universal parameters adjusted to data, this approach has achieved a high level of accuracy in the description of structure properties over the whole chart of nuclides, from relatively light systems to superheavy nuclei, and from the valley of β stability to the particle drip lines.

In this work we introduce a fully self-consistent microscopic framework for the calculation of weak-interaction rates at finite temperature, based on Skyrme functionals. The single-nucleon basis and the corresponding thermal occupation factors of the initial nuclear state are determined in the finite-temperature Skyrme Hartree-Fock model, and charge-exchange transitions to excited states are computed using the finite-temperature RPA. Effective interactions are implemented self-consistently, meaning both the finite-temperature single-nucleon Hartree-Fock equations and the matrix equations of the RPA are based on the same Skyrme energy density functional. The advantage of this approach over shell-model calculations or hybrid models is that a particular finite-temperature Hartree-Fock plus RPA model (i.e., one determined completely by the choice of a Skyrme functional) can be extended over arbitrary mass regions of the nuclide chart without additional assumptions or adjustment of parameters, as for instance single-particle energies, to transitions within specific shells. In a simple RPA, of course, correlations are described only on the one-particle, one-hole level; therefore, one cannot expect the model to reproduce the details of the fragmentation of GT strength distributions. This can be accomplished only in the shell-model approach, which includes higher order correlations. In general, however, the RPA reproduces the centroid of strength distributions and the total GT strength. For electron capture particularly, the RPA is an appropriate tool for the evaluation of cross sections for capture on nuclei under conditions where the electron chemical potentials are larger than the characteristic nuclear Q values [3].

Rather than evaluating and tabulating weak-interaction rates for hundreds of nuclei already at this stage, in the present work we perform illustrative calculations of electron-capture cross sections for selected nuclei in the iron mass group and for neutron-rich Ge isotopes and compare results with those obtained with the SMMC approach [9] and the hybrid SMMC/RPA model [10], respectively. Calculations are performed for a representative set of Skyrme functionals, and this provides an estimate of the range of theoretical uncertainty inherent in the Skyrme Hartree-Fock plus RPA approach.

The framework of finite-temperature Skyrme Hartree-Fock plus charge-exchange RPA and the formalism for calculating cross sections for electron capture are introduced in Sec. II. Electron capture on iron-group nuclei ($A \approx 45$–65) is considered in Sec. III and cross sections for electron capture on neutron-rich Ge isotopes are evaluated in Sec. IV. Section V summarizes the results of the present investigations and concludes with an outlook for future studies.

II. CALCULATION OF ELECTRON-CAPTURE CROSS SECTIONS WITH FINITE-TEMPERATURE SKYRME HARTREE-FOCK PLUS RPA

A. Charge-exchange RPA at finite temperature

Throughout presupernova evolution, electron capture on nuclei proceeds at finite temperature. In addition to capture on pf-shell nuclei, this process also takes place on neutron-rich nuclei with protons in the pf shell and neutron number $N > 40$. Finite-temperature effects and correlations unblock GT transitions that are forbidden at zero temperature.

In the present analysis we employ the fully self-consistent finite-temperature charge-exchange random-phase approximation (FTRPA), formulated in the single-nucleon basis of the Skyrme Hartree-Fock model at finite temperature (FTSHF). Effective interactions are implemented self-consistently, meaning both the FTSHF equations and the matrix equations of FTRPA are based on the same Skyrme energy density functional. For a description of open-shell nuclei it is also necessary to include a consistent treatment of pairing correlations like, for instance, in the finite-temperature

Hartree-Fock-Bogoliubov plus quasiparticle random-phase approximation (HFB + QRPA) framework [15,16]. However, in nuclei the phase transition from a superfluid to normal state occurs at temperatures $T \approx 0.5$–1 MeV [17–19], whereas for temperatures above $T \approx 4$ MeV, contributions from states in the continuum become large, and additional subtraction schemes have to be implemented to remove the contributions of the external nucleon gas [20]. In this work we consider a range of temperatures relevant for the stellar electron-capture process, $T = 0.5$–1.5 MeV [10], for which the FTSHF plus FTRPA should provide an accurate description of the GT and forbidden transitions.

The finite-temperature Hartree-Fock (HF) framework [20,21] has been successfully used in nuclear-structure calculations for many years. In the case of a Skyrme functional the finite-temperature HF equations have the same form as at zero temperature, but the density reads

$$\rho(\vec{r}) = \sum_{\alpha} f_{\alpha} \phi^{*}_{\alpha}(\vec{r}) \phi_{\alpha}(\vec{r}), \tag{3}$$

where, in addition to bilinear products of single-nucleon HF wave functions ϕ_{α}, the contribution of each single-nucleon state is determined by the Fermi-Dirac (FD) occupation factors,

$$f_{\alpha} = \frac{1}{1 + e^{(1/kT)(\epsilon_{\alpha} - \mu)}}, \tag{4}$$

where ϵ_{α} are the single-nucleon energies and the chemical potential μ is determined by the conservation of the number of nucleons, $\sum_{\alpha} f_{\alpha} = A$. In this sense the implementation of the finite-temperature formalism is very similar to the treatment of pairing correlations in the BCS framework, with FD factors replacing the occupancies v^2_{α}. The FD factors determine contributions from individual single-nucleon states to other types of densities as well (e.g., kinetic energy density and spin-orbit density).

A detailed derivation of the (Q)RPA formalism at finite temperature can be found in Refs. [15,22–24] and the first self-consistent extension to open-shell nuclei (finite-temperature QRPA) has been reported recently in Ref. [16]. Finite-temperature linear response theory and RPA have been successfully used in numerous studies of giant resonances and decay of hot nuclei [15,20,22–31]. The FTRPA represents the small-amplitude limit of the time-dependent mean-field theory at finite temperature. Starting from the response of a time-dependent density matrix $\rho(t)$ to a harmonic external field $f(t)$ [32], the equation of motion for the density operator reads

$$i\,\partial_t \hat{\rho} = [\hat{h}[\hat{\rho}] + \hat{f}(t), \hat{\rho}]. \tag{5}$$

In the small-amplitude limit the density matrix is expanded to linear order,

$$\hat{\rho}(t) = \hat{\rho}^0 + \delta\hat{\rho}(t), \tag{6}$$

where

$$\delta\hat{\rho}(t) = \delta\hat{\rho}^{(+)} e^{-i\omega t} + \delta\hat{\rho}^{(-)} e^{+i\omega t}, \tag{7}$$

and $\hat{\rho}^0$ denotes the stationary ground-state density,

$$\rho^0_{\alpha\beta} = \delta_{\alpha\beta} f_{\alpha} = \delta_{\alpha\beta}[1 + e^{(1/kT)(\epsilon_{\alpha} - \mu)}]^{-1}, \tag{8}$$

and includes the thermal occupation factors of single-particle states f_k. For the analogous expansion of the Hamiltonian operator $\hat{h}(t) = \hat{h}^{(0)} + \delta\hat{h}(t)$, the linearized equation of motion reads

$$i\hbar\,\partial_t \delta\hat{\rho} = [\hat{h}^{(0)}, \delta\hat{\rho}] + \left[\frac{\delta\hat{h}}{\delta\rho}\delta\hat{\rho}, \hat{\rho}^{(0)}\right]. \tag{9}$$

Taking the matrix elements of this equation between the states $\langle\alpha\beta^{-1}|$ and $|0\rangle$, we obtain

$$\begin{aligned}
\hbar\omega\delta\rho^{(+)}_{\alpha\beta} &= (\epsilon_{\alpha} - \epsilon_{\beta})\delta\rho^{(+)}_{\alpha\beta} + \sum_{\gamma\delta}(f_{\delta} - f_{\gamma}) v_{\alpha\bar{\delta}\bar{\beta}\gamma}\delta\rho^{(+)}_{\gamma\delta} \\
&\quad + (f_{\gamma} - f_{\delta}) v_{\alpha\gamma\bar{\beta}\bar{\delta}}\delta\rho^{(-)}_{\gamma\delta}, \\
-\hbar\omega\delta\rho^{(-)}_{\alpha\beta} &= (\epsilon_{\alpha} - \epsilon_{\beta})\delta\rho^{(-)}_{\alpha\beta} + \sum_{\gamma\delta}(f_{\gamma} - f_{\delta}) v_{\alpha\gamma\bar{\beta}\bar{\delta}}\delta\rho^{(+)}_{\gamma\delta} \\
&\quad + (f_{\delta} - f_{\gamma}) v_{\alpha\bar{\delta}\bar{\beta}\gamma}\delta\rho^{(-)}_{\gamma\delta},
\end{aligned} \tag{10}$$

for terms multiplying the factors $e^{-i\omega t}$ and $e^{+i\omega t}$, respectively, and

$$\delta h^{(+)}_{\alpha\beta} = \sum_{\gamma\delta}(f_{\delta} - f_{\gamma}) v_{\alpha\bar{\delta}\bar{\beta}\gamma}\delta\rho^{(+)}_{\gamma\delta} + (f_{\gamma} - f_{\delta}) v_{\alpha\gamma\bar{\beta}\bar{\delta}}\delta\rho^{(-)}_{\gamma\delta}, \tag{11}$$

and analogously for $\delta h^{(-)}_{\alpha\beta}$. These relations are consistent with the definition of the HF mean field at finite temperature and express the fact that thermal occupancies determine the way density fluctuations affect the mean field. Equations (10) are consistent with those defined in Ref. [22]. If the first (second) equation of the set (10) is multiplied by $f_{\beta} - f_{\alpha}$ ($f_{\alpha} - f_{\beta}$), with the definition $F_{\alpha\beta} = \delta\rho^{(+)}_{\alpha\beta}$ and $F_{\beta\alpha} = \delta\rho^{(-)}_{\alpha\beta}$, then Eqs. (10) take the form as in Ref. [23]. The set of Eqs. (10) is also consistent with the derivation of finite-temperature QRPA in Ref. [15] in the limit of vanishing pairing correlations. However, in Ref. [15] a different definition of the RPA amplitudes, which involves such quantities as $\sqrt{f_{\alpha} - f_{\beta}}$, is introduced. This requires special care in the proton-neutron case because no simple condition that would guarantee that the quantity under the square root is positive can be imposed.

The finite-temperature forward- and backward-going amplitudes can be related to the corresponding zero-temperature amplitudes (X and Y) through the following relations:

$$\delta\rho^{(+)}_{\alpha\beta} = X_{\alpha\beta} f_{\beta}(1 - f_{\alpha}) + Y_{\beta\alpha} f_{\alpha}(1 - f_{\beta}) \tag{12}$$

and

$$\delta\rho^{(-)}_{\alpha\beta} = Y_{\alpha\beta} f_{\beta}(1 - f_{\alpha}) + X_{\beta\alpha} f_{\alpha}(1 - f_{\beta}). \tag{13}$$

The charge-exchange RPA matrices are composed of matrix elements of the residual interaction v, as well as certain combinations of thermal occupation factors f_k. Because of finite temperature, the configuration space includes particle-hole (ph), particle-particle (pp), and hole-hole (hh) proton-neutron pairs. The residual interaction is derived from a Skyrme energy density functional and single-particle occupation factors at finite temperature are included in a consistent way in both the FTSHF and the FTRPA. The same interaction is used in both the FTSHF equations that determine the single-nucleon basis

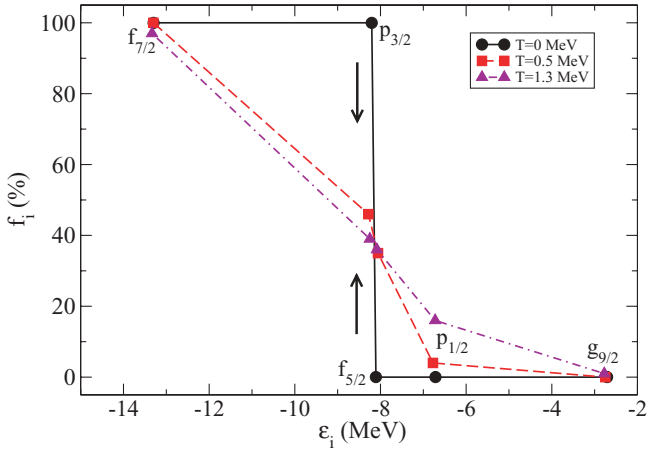

FIG. 1. (Color online) Occupation percentage of the proton orbitals $f_{7/2}$, $p_{3/2}$, $f_{5/2}$, $p_{1/2}$, and $g_{9/2}$ in ^{74}Ge, calculated in the finite-temperature Skyrme HF model with the SGII interaction, at zero temperature, $T = 0.5$ MeV, and $T = 1.3$ MeV.

and the matrix equations of the FTRPA. The full set of FTRPA equations is solved by diagonalization. The result is excitation energies and the corresponding forward- and backward-going amplitudes that are used to evaluate the transition strength for a given multipole operator.

As an illustrative example, in Figs. 1 and 2 we display the temperature dependence of the occupations of the proton and neutron orbitals $f_{7/2}$, $p_{3/2}$, $f_{5/2}$, $p_{1/2}$, and $g_{9/2}$ in ^{74}Ge, calculated using the FTSHF model. The self-consistent calculation with the SGII effective interaction [33] corresponds to zero temperature, $T = 0.5$ MeV, and $T = 1.3$ MeV. At zero temperature the proton orbitals $f_{7/2}$ and $p_{3/2}$ are fully occupied, whereas $f_{5/2}$, $p_{1/2}$, and $g_{9/2}$ are empty. By increasing the temperature, protons are mostly promoted from the $p_{3/2}$ orbital into the $f_{5/2}$ orbital and, to a lesser extent, into the $p_{1/2}$ orbital. Correspondingly, the occupation percentage of $p_{3/2}$ is reduced, whereas those of the $f_{5/2}$ and $p_{1/2}$ orbitals are enhanced. In the temperature intervals considered here, the occupations of the $f_{7/2}$ and $g_{9/2}$ orbitals do not change significantly. At zero temperature neutrons fully occupy the $f_{7/2}$, $p_{3/2}$, $f_{5/2}$, and $p_{1/2}$ orbitals and there are two neutrons in the $g_{9/2}$ orbital. The main effect of increasing temperature is to promote neutrons from the $p_{3/2}$, $f_{5/2}$, and $p_{1/2}$ orbitals into the $g_{9/2}$ orbital. Note, however, that for protons already at $T = 0.5$ MeV the calculation predicts a pronounced effect on the occupation of orbitals close to the Fermi surface, whereas the occupation of neutron orbitals is modified significantly only at the higher temperature of $T = 1.3$ MeV. The results shown in Figs. 1 and 2 can be compared to thermal occupation numbers calculated from canonical SMMC in Ref. [10], with Woods-Saxon single-particle energies and a pairing plus quadrupole residual interaction. The temperature dependence of occupation numbers predicted by the two models is similar, with the SMMC results showing a more pronounced effect on occupation numbers already at $T = 0.5$ MeV, especially for neutron orbitals. This can be attributed to a smaller energy gap between the $p_{1/2}$ and the $g_{9/2}$ single-neutron orbitals used in the SMMC calculation and to additional correlations in the ground state that are not taken into account in the simple Skyrme HF model.

In Fig. 3 we display the temperature dependence of the corresponding GT$^-$ and GT$^+$ strength distributions in ^{74}Ge, calculated with the finite-temperature proton-neutron RPA model based on the Skyrme SGII interaction. In the GT$^-$ direction a neutron is changed into a proton, as in β decay. At low temperature the GT$^-$ mode corresponds to a coherent superposition of $J^\pi = 1^+$ charge-exchange proton-particle, neutron-hole transitions. The GT operator reads

$$T^{\pm}_{\mathrm{GT}} = \sum_{i=1}^{A} \boldsymbol{\sigma}\tau_{\pm}. \tag{14}$$

In addition to the high-energy GT$^-$ resonance at ≈14 MeV, a collective superposition of direct spin-flip ($j = l + \frac{1}{2} \rightarrow j = l - \frac{1}{2}$) transitions, the response function displays a

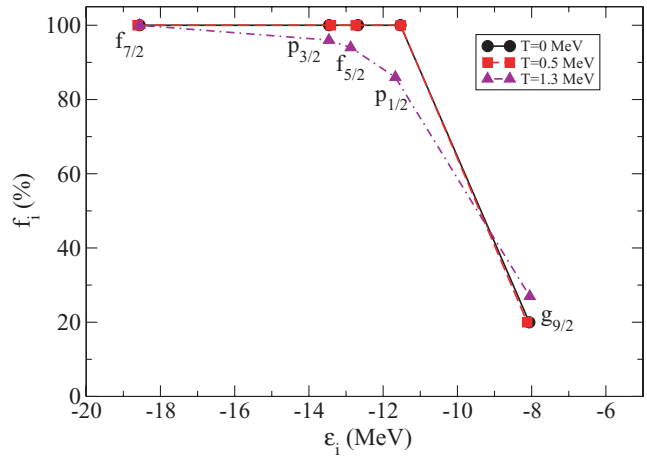

FIG. 2. (Color online) Occupation percentage of the neutron orbitals $f_{7/2}$, $p_{3/2}$, $f_{5/2}$, $p_{1/2}$, and $g_{9/2}$ in ^{74}Ge, calculated in the finite-temperature Skyrme HF model with the SGII interaction, at zero temperature, $T = 0.5$ MeV, and $T = 1.3$ MeV.

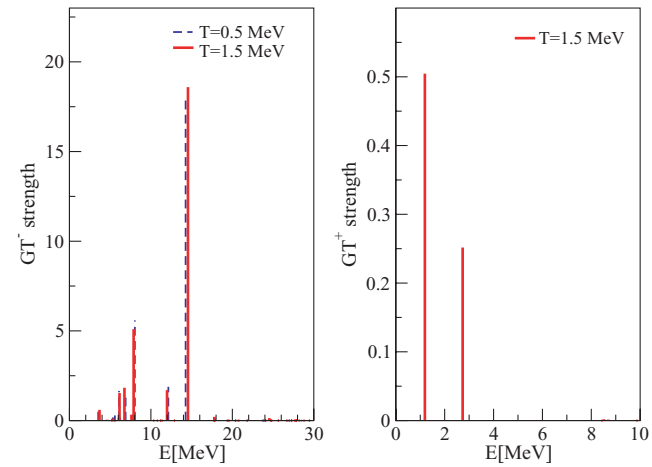

FIG. 3. (Color online) Temperature dependence of GT$^-$ and GT$^+$ strength distributions in ^{74}Ge, calculated with the finite-temperature proton-neutron RPA model based on the Skyrme SGII interaction.

concentration of strength in the low-energy tail. The transitions in the low-energy region correspond to core-polarization ($j = l \pm \frac{1}{2} \rightarrow j = l \pm \frac{1}{2}$) and back spin-flip ($j = l - \frac{1}{2} \rightarrow j = l + \frac{1}{2}$) neutron-hole, proton-particle excitations. The GT$^-$ transitions are allowed at $T = 0$ and the distribution displays only a weak temperature dependence. However, for ^{74}Ge the GT$^+$ transitions, in which a proton is changed into a neutron, are forbidden at zero temperature because the relevant neutron orbitals are fully occupied. Note that additional ground-state correlations (e.g., pairing) are not taken into account in the Skyrme HF + RPA model. Even at $T = 0.5$ MeV the occupation factors of neutron orbitals remain unchanged (cf. Fig. 2) and the calculation does not predict any low-energy GT$^+$ transition. Only at higher temperatures above $T = 1.0$ MeV are the low-energy GT$^+$ transitions thermally unblocked. We have verified that at each temperature the GT strength distribution satisfies the Ikeda sum rule [34],

$$(S^-_{\rm GT} - S^+_{\rm GT}) = 3(N - Z), \tag{15}$$

where $S^\pm_{\rm GT}$ denotes the total sum of GT strength for the GT$^\pm$ transitions.

B. Cross section for electron capture

The electron capture on a nucleus (Z, N),

$$e^- + (Z, N) \longrightarrow \nu_e + (Z - 1, N + 1)^*, \tag{16}$$

presents a simple semileptonic reaction that proceeds via the charged current of the weak interaction. Theoretical analysis of these processes necessitates the description of the weak interaction between leptons and nucleons, as well as the wave functions of the initial and final nuclear states. Detailed expressions for the reaction rates and the transition matrix elements can be found in Refs. [35–37]. The electron-nucleus reaction cross section for a transition between the states $|i\rangle$ and $|f\rangle$ reads

$$\frac{d\sigma}{d\Omega} = \frac{V E_\nu^2}{(2\pi)^2} \sum_{\text{lepton spins}} \frac{1}{2J_i + 1} \sum_{M_i} \sum_{M_f} |\langle f|\, \hat{H}_W\, |i\rangle|^2, \tag{17}$$

where V denotes the quantization volume and E_ν is the energy of the outgoing electron neutrino. The Hamiltonian $\hat{H}_W$ of the weak interaction is expressed in the standard current-current form, that is, in terms of the nucleon $\mathcal{J}_\lambda(\boldsymbol{x})$ and lepton $j_\lambda(\boldsymbol{x})$ currents,

$$\hat{H}_W = -\frac{G}{\sqrt{2}} \int d^3x \mathcal{J}_\lambda(\boldsymbol{x}) j^\lambda(\boldsymbol{x}), \tag{18}$$

where G is the weak coupling constant and the resulting transition matrix element reads

$$\langle f|\hat{H}_W|i\rangle = -\frac{G}{\sqrt{2}} l_\lambda \int \frac{d^3x}{1/\sqrt{V}} e^{-i\boldsymbol{q}\cdot\boldsymbol{x}} \langle f|\mathcal{J}^\lambda(\boldsymbol{x})|i\rangle, \tag{19}$$

where the four-momentum transfer is $q \equiv (q_0, \boldsymbol{q})$ and the multipole expansion of the leptonic matrix element $l_\lambda e^{-i\boldsymbol{q}\cdot\boldsymbol{x}}$ determines the operator structure for the nuclear transition matrix elements [35–37]. The expression for the electron-capture cross sections is given by

$$\begin{aligned}\frac{d\sigma}{d\Omega} = {} & \frac{G_F^2 \cos^2\theta_c}{2\pi} \frac{F(Z, E_e)}{(2J_i + 1)} \\ & \times \Bigg(\sum_{J \geqslant 1} \mathcal{W}(E_\nu) \big\{ (1 - (\hat{\boldsymbol{\nu}} \cdot \hat{\boldsymbol{q}})(\boldsymbol{\beta} \cdot \hat{\boldsymbol{q}})) \\ & \times \left[\left| \langle J_f || \hat{\mathcal{T}}^{\rm mag}_J || J_i \rangle \right|^2 + \left| \langle J_f || \hat{\mathcal{T}}^{\rm el}_J || J_i \rangle \right|^2 \right] \\ & - 2\hat{\boldsymbol{q}} \cdot (\hat{\boldsymbol{\nu}} - \boldsymbol{\beta}) \mathrm{Re} \langle J_f || \hat{\mathcal{T}}^{\rm mag}_J || J_i \rangle \langle J_f || \hat{\mathcal{T}}^{\rm el}_J || J_i \rangle^* \big\} \\ & + \sum_{J \geqslant 0} \mathcal{W}(E_\nu) \{ (1 - \hat{\boldsymbol{\nu}} \cdot \boldsymbol{\beta}) + 2(\hat{\boldsymbol{\nu}} \cdot \hat{\boldsymbol{q}})(\boldsymbol{\beta} \cdot \hat{\boldsymbol{q}}) \\ & \times \langle J_f || \hat{\mathcal{L}}_J || J_i \rangle|^2 + (1 + \hat{\boldsymbol{\nu}} \cdot \boldsymbol{\beta}) \langle J_f || \hat{\mathcal{M}}_J || J_i \rangle|^2 \\ & - 2\hat{\boldsymbol{q}}(\hat{\boldsymbol{\nu}} + \boldsymbol{\beta}) \mathrm{Re} \langle J_f || \hat{\mathcal{L}}_J || J_i \rangle \langle J_f || \hat{\mathcal{M}}_J || J_i \rangle^* \} \Bigg), \end{aligned} \tag{20}$$

where the momentum transfer $\boldsymbol{q} = \boldsymbol{\nu} - \boldsymbol{k}$ is defined as the difference between neutrino and electron momenta, $\hat{\boldsymbol{q}}$ and $\hat{\boldsymbol{\nu}}$ are the corresponding unit vectors, and $\boldsymbol{\beta} = \boldsymbol{k}/E_e$. The energies of the incoming electron and outgoing neutrino are denoted by E_e and E_ν, respectively. The Fermi function $F(Z, E_e)$ corrects the cross section for the distortion of the electron wave function by the Coulomb field of the nucleus [38].

$$\mathcal{W}(E_\nu) = \frac{E_\nu^2}{(1 + E_\nu/M_T)}, \tag{21}$$

where the phase-space factor $(1 + E_\nu/M_T)^{-1}$ accounts for nuclear recoil and M_T is the mass of the target nucleus. The nuclear transition matrix elements between the initial state $|J_i\rangle$ and the final state $|J_f\rangle$ correspond to the charge $\hat{\mathcal{M}}_J$, longitudinal $\hat{\mathcal{L}}_J$, transverse electric $\hat{\mathcal{T}}^{\rm el}_J$, and transverse magnetic $\hat{\mathcal{T}}^{\rm mag}_J$ multipole operators:

(i) the Coulomb operator,

$$\begin{aligned}\hat{\mathcal{M}}_{JM}(\boldsymbol{x}) = {} & F_1^V M_J^M(\boldsymbol{x}) - i\frac{\kappa}{m_N} \\ & \times \left[F_A \Omega_J^M(\boldsymbol{x}) + \frac{1}{2}(F_A - m_e F_P) \Sigma''^M_J(\boldsymbol{x}) \right], \end{aligned} \tag{22}$$

(ii) the longitudinal operator,

$$\hat{\mathcal{L}}_{JM}(\boldsymbol{x}) = \frac{q_0}{\kappa} F_1^V M_J^M(\boldsymbol{x}) + i F_A \Sigma''^M_J(\boldsymbol{x}), \tag{23}$$

(iii) the transverse electric operator,

$$\begin{aligned}\hat{\mathcal{T}}^{\rm el}_{JM}(\boldsymbol{x}) = {} & \frac{\kappa}{m_N} \left[F_1^V \Delta'^M_J(\boldsymbol{x}) + \frac{1}{2}\mu^V \Sigma^M_J(\boldsymbol{x}) \right] \\ & + i F_A \Sigma'^M_J(\boldsymbol{x}), \text{ and} \end{aligned} \tag{24}$$

(iv) the transverse magnetic operator,

$$\begin{aligned}\hat{\mathcal{T}}^{\rm mag}_{JM}(\boldsymbol{x}) = {} & -i\frac{\kappa}{m_N} \left[F_1^V \Delta^M_J(\boldsymbol{x}) - \frac{1}{2}\mu^V \Sigma'^M_J(\boldsymbol{x}) \right] \\ & + F_A \Sigma^M_J(\boldsymbol{x}), \end{aligned} \tag{25}$$

where all the form factors are functions of q^2 and $\kappa = |\boldsymbol{q}|$. The operators M, Ω, Δ, Δ', Σ, Σ', and Σ'' are expressed in terms of spherical Bessel functions, spherical harmonics, and vector spherical harmonics [35]. By assuming conserved vector current, the standard set of form factors reads [39]

$$F_1^V(q^2) = \left[1 + \left(\frac{q}{840\ \text{MeV}}\right)^2\right]^{-2}, \tag{26}$$

$$\mu^V(q^2) = 4.706\left[1 + \left(\frac{q}{840\ \text{MeV}}\right)^2\right]^{-2}, \tag{27}$$

$$F_A(q^2) = -1.262\left[1 + \left(\frac{q}{1032\ \text{MeV}}\right)^2\right]^{-2}, \tag{28}$$

$$F_P(q^2) = \frac{2m_N F_A(q^2)}{q^2 + m_\pi^2}. \tag{29}$$

The cross sections for electron capture are evaluated from Eq. (20), with transition matrix elements between the initial and final states determined in a self-consistent microscopic framework based on the (finite-temperature) Skyrme HF model for the nuclear ground state and excited states calculated using the corresponding (finite-temperature) RPA. For each transition operator $\hat{O}_J$ the matrix elements between the initial state of the even-even (Z, N) target nucleus and the final state in the corresponding $(Z-1, N+1)$ nucleus are expressed in terms of single-particle matrix elements between the single-nucleon states and the corresponding (finite-temperature) RPA amplitudes $\delta\rho_{\alpha\beta}^{(+)J}$ and $\delta\rho_{\alpha\beta}^{(-)J}$ (cf. Sec. II A):

$$\langle J_f||\hat{O}_J||J_i\rangle = \sum_{\alpha\beta}\langle\alpha||\hat{O}_J||\beta\rangle\left(\delta\rho_{\alpha\beta}^{(+)J} - \delta\rho_{\alpha\beta}^{(-)J}\right). \tag{30}$$

The energy of the outgoing neutrino is determined by the conservation relation

$$E_\nu = E_e - Q + E_i - E_f, \tag{31}$$

which includes the difference between the final and the initial nuclear states. The Q value plays a particularly important role in the calculation of electron-capture rates. Namely, the energy that is available to excite states in the daughter nucleus depends on whether electron capture on a specific target nucleus releases energy ($Q < 0$) or requires an additional external input ($Q > 0$). In the present calculation the Q value is determined from the experimental masses [40]: $Q = M_f - M_i$, where $M_{i,f}$ are the masses of the parent and daughter nuclei, respectively.

The nuclei that will be considered in this work contribute to stellar electron-capture rates in the temperature interval $T \approx$ 0.5–1.5 MeV [10]. The expression for the total cross section for electron capture on a nucleus (Z, N) at temperature T reads

$$\sigma(E_e, T) = \frac{G^2}{2\pi}\sum_i F(Z, E_e)\frac{(2J_i+1)e^{-E_i/(kT)}}{G(Z, A, T)} \times \sum_{f,J}(E_e - Q + E_i - E_f)^2\frac{|\langle i|\hat{O}_J|f\rangle|^2}{(2J_i+1)}, \tag{32}$$

where $\hat{O}_J$ is the generic notation for the charge $\hat{\mathcal{M}}_J$, longitudinal $\hat{\mathcal{L}}_J$, transverse electric $\hat{\mathcal{T}}_J^{\text{el}}$, and transverse magnetic $\hat{\mathcal{T}}_J^{\text{mag}}$ multipole operators. The sum over initial states includes a thermal average of levels, with the corresponding partition function $G(Z, A, T)$. The finite temperature induces the thermal population of excited states in the parent nucleus. Each of these states $|i\rangle$ is connected by the multipole operators to many levels $|f\rangle$ in the daughter nucleus. The calculation of all possible transitions is computationally prohibitive; therefore, the evaluation of the total cross section for electron capture is usually simplified [5,6,10,41] by adopting the Brink hypothesis, that is, by assuming that the strength distribution of the multipole operators in the daughter nucleus is the same for all initial states and shifted by the excitation energy of the initial state. By using this approximation, the sum over final states becomes independent of the initial state and the sum over the Boltzmann weights cancels the partition function. The Brink hypothesis is a valid approximation when the temperature and density are high enough that many states contribute and variations in the low-energy transition strength cancel out. As was done in the calculation of stellar electron capture on neutron-rich germanium isotopes in Ref. [10], we apply the Brink hypothesis to the initial state, which represents the thermal average of many-body states in the parent nucleus at temperature T. This thermally averaged initial state is approximated by the FTSHF ground-state Slater determinant with FD thermal occupation factors. With this approximation the final expression for the total electron-capture cross section at temperature T reads

$$\sigma(E_e, T) = \frac{G^2}{2\pi}F(Z, E_e) \times \sum_f(E_e - Q - \omega_f)^2\sum_J S_J(\omega_f, T), \tag{33}$$

where ω_f is the excitation energy in the daughter nucleus and S_J is the discrete finite-temperature RPA response for the multipole operator $\hat{O}_J$.

III. ELECTRON CAPTURE ON IRON-GROUP NUCLEI

As our first illustrative example and application of the model, we consider electron capture on iron-group nuclei ($A \approx$ 45–65). The calculated electron-capture cross sections and rates for nuclei in this mass range are essential for modeling the initial phase of stellar core collapse and supernova explosion [1–3,41]. In the presupernova collapse, electron capture on pf-shell nuclei proceeds at temperatures between 300 and 800 keV. Detailed calculations of stellar weak-interaction rates in the iron mass region have been carried out in the framework of the interacting shell model [2]. Both SMMC [9] and large-scale shell-model diagonalization [6,7] were used to calculate electron capture and β-decay rates in the $A \approx$ 45–65 mass region. The SMMC results [9] were, in fact, superseded in Ref. [6] by the weak-interaction rates obtained using large-scale shell-model diagonalization in the complete pf shell.

In this section we calculate electron-capture cross sections for selected nuclei in the iron mass region and compare the results with those in Ref. [9], where the SMMC was used to

calculate GT^+ strength distributions (where in this direction a proton is changed into a neutron) and these distributions were then used to compute the electron-capture cross sections and rates in the zero-momentum transfer limit as a function of the incident energy of the electron. The SMMC calculations solve the full shell-model problem for the GT^+ strength distributions in the $0\hbar\omega$ fp-shell space using a realistic residual interaction. In the calculation in Ref. [9] the KB3 residual interaction [42] was used and the quenching of the total GT strength was taken into account by renormalizing the GT transition matrix elements by the constant factor 0.8. In the present analysis the cross sections for electron capture are evaluated using Eq. (33), with transition matrix elements between the initial and final states determined in the self-consistent microscopic framework based on the FTSHF model for the nuclear ground state and excited states calculated using the corresponding FTRPA.

In Fig. 4 we display the calculated cross sections for the reaction $^{56}\mathrm{Fe}(e^-,\nu_e)^{56}\mathrm{Mn}$ as functions of the incident electron energy E_e. Calculations are performed at temperature $T = 0.5$ MeV and the Skyrme HF + RPA results are compared with cross sections calculated using SMMC GT strength distributions [9]. Because the calculation of cross sections in Ref. [9] corresponds to the zero-momentum transfer limit and includes only the GT operator, for the sake of comparison we have also limited the sum in Eq. (20) to the 1^+ channel (i.e., only transitions to 1^+ excited states are taken into account). At low momentum transfer, the allowed GT transitions dominate the electron-capture process on pf-shell nuclei. Note, however, that in the calculation of Dean *et al.* [9] only the $0\hbar\omega$ GT transition strength is considered, rather than the total strength in the 1^+ channel. The reduction of the axial-vector coupling constant from its free-nucleon value $g_A = 1.262$ to $g_A = 1.0$ [cf. Eq. (28)] is equivalent to the renormalization of the GT matrix elements in Ref. [9] by the constant factor 0.8. In the shell-model studies of weak-interaction rates in the $A \approx 45$–65 mass region, both the SMMC [9] and the shell-model diagonalization approach [6] have used the KB3 residual interaction, which is well suited for full $0\hbar\omega$ calculations throughout the lower pf-shell region. However, to calculate the weak-interaction rates in the entire mass range $A \approx 45$–65, the original KB3 interaction had to be modified by including a number of monopole corrections to reproduce the GT strength distributions and half-lives.

In the present analysis, the cross sections, as functions of the incident electron energy, are computed for a representative set of Skyrme functionals: SGII [33], SkM* [43], SLy4 [44], SLy5 [45], and SkO′ [46]. Over the past 30 years, more than 100 different Skyrme parametrizations have been adjusted and analyzed and it is often difficult to compare results obtained with different models because they can include different subsets of terms from the most general functional. Because in this work we apply the microscopic approach based on Skyrme HF + RPA model, calculations are performed using various Skyrme functionals. In principle, this will provide an estimate of the range of theoretical uncertainty inherent in the present approach. The electron-capture cross sections in Fig. 4 exhibit a sharp increase of several orders of magnitude within the first few MeV above threshold, and this reflects the GT^+ distributions. For electron energy $E_e \geqslant 10$ MeV the calculated cross sections display a more gradual increase. A very similar energy dependence of the cross sections is

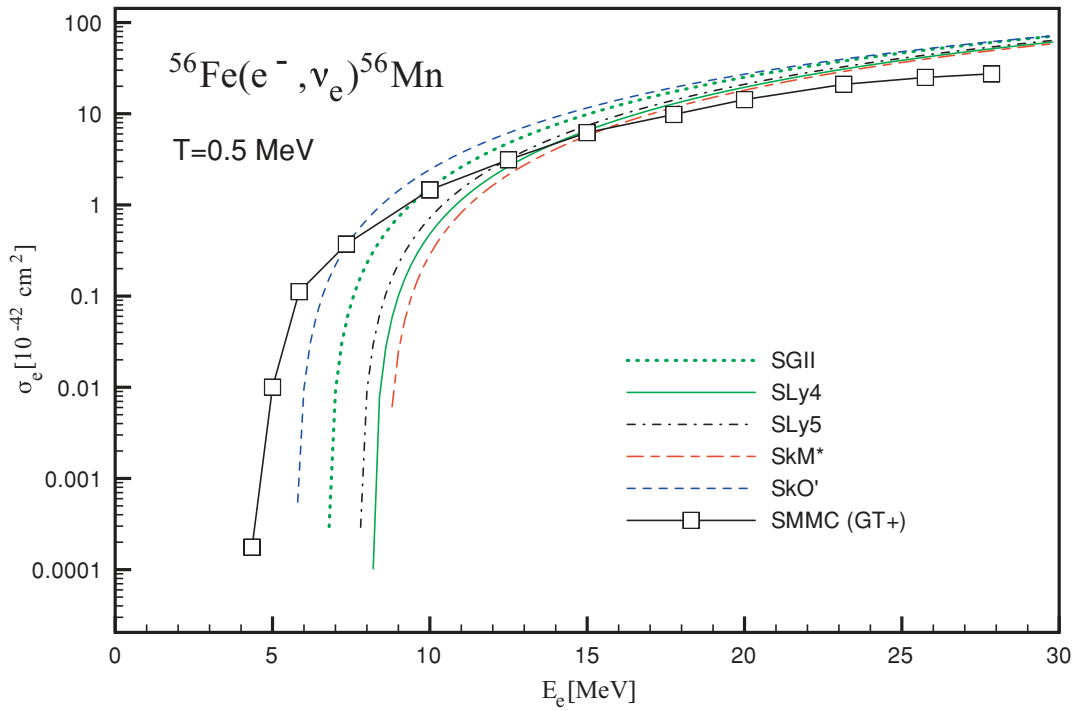

FIG. 4. (Color online) Electron-capture cross sections for the reaction $^{56}\mathrm{Fe}(e^-,\nu_e)^{56}\mathrm{Mn}$ at $T = 0.5$ MeV as functions of the incident electron energy E_e. The Skyrme HF + RPA results are compared with cross sections calculated from the SMMC GT strength distributions [9].

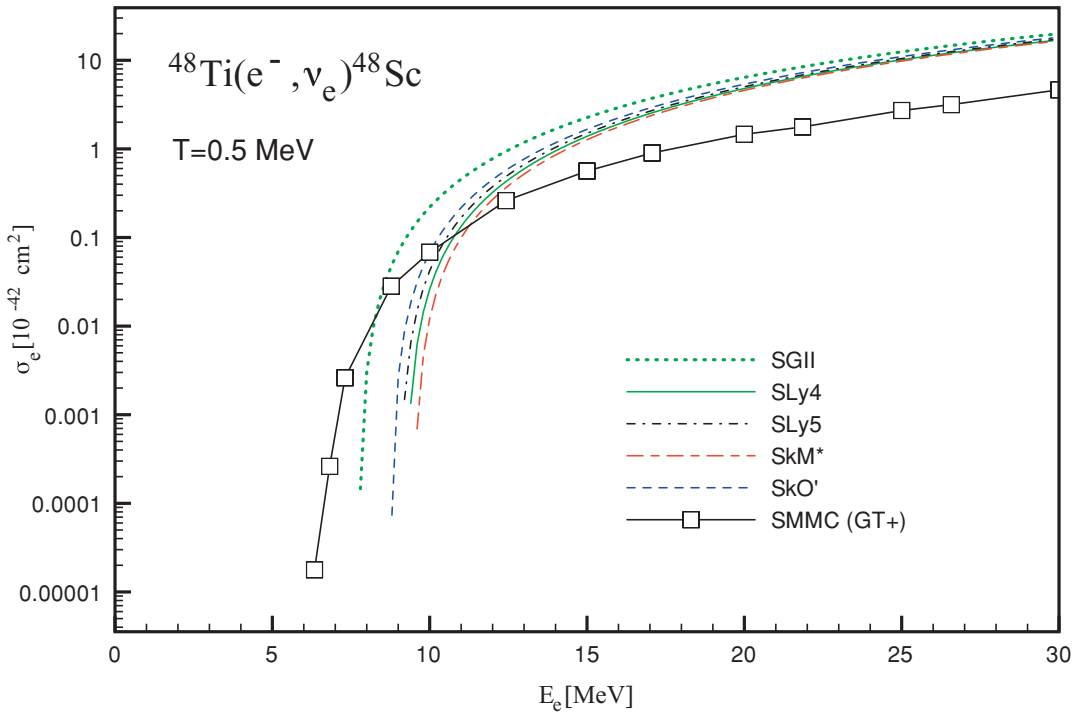

FIG. 5. (Color online) Same as Fig. 4, but for the reaction ^{48}Ti$(e^-,\nu_e)^{48}$Sc.

calculated for the neighboring even-even parent nuclei ^{48}Ti and ^{50}Cr, in Figs. 5 and 6, respectively. At low energies all Skyrme HF + RPA cross sections are below the values based on SMMC calculations. This is especially pronounced in ^{56}Fe$(e^-,\nu_e)^{56}$Mn and much less in ^{50}Cr$(e^-,\nu_e)^{50}$V. Cross sections calculated at very low electron energies will be very sensitive to the discrete level structure of the GT transitions. These cross sections, however, are several orders of magnitude smaller than those for $E_e \geqslant 10$ MeV and, when folded with the electron flux to calculate capture rates, the differences between

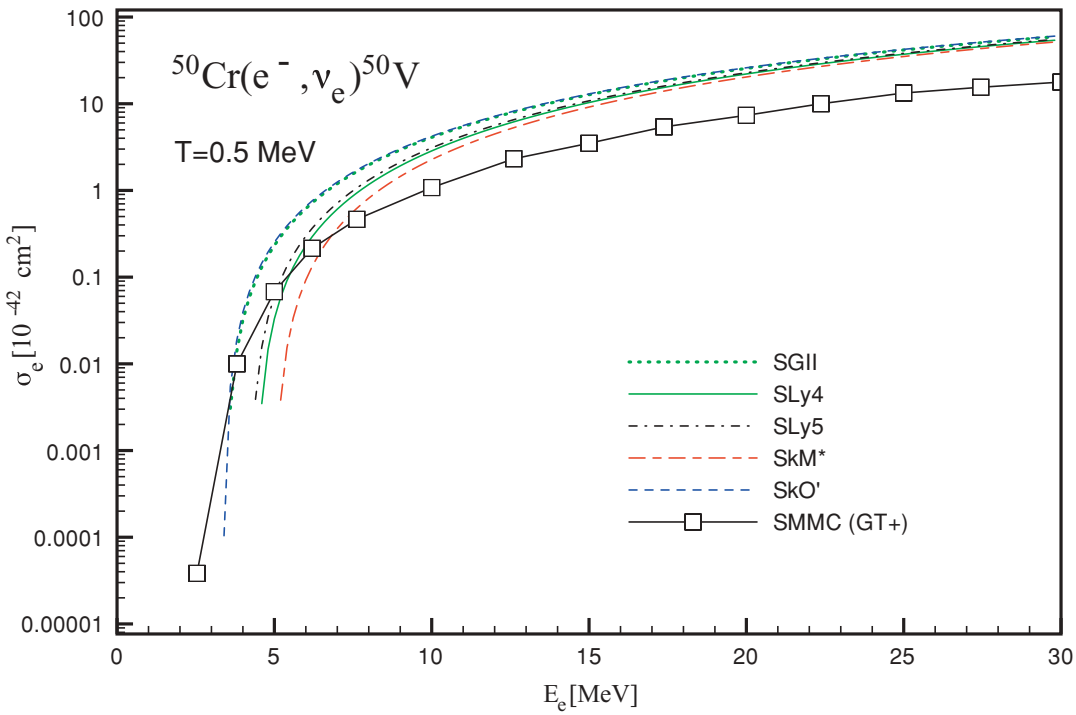

FIG. 6. (Color online) Same as Fig. 4, but for the reaction ^{50}Cr$(e^-,\nu_e)^{50}$V.

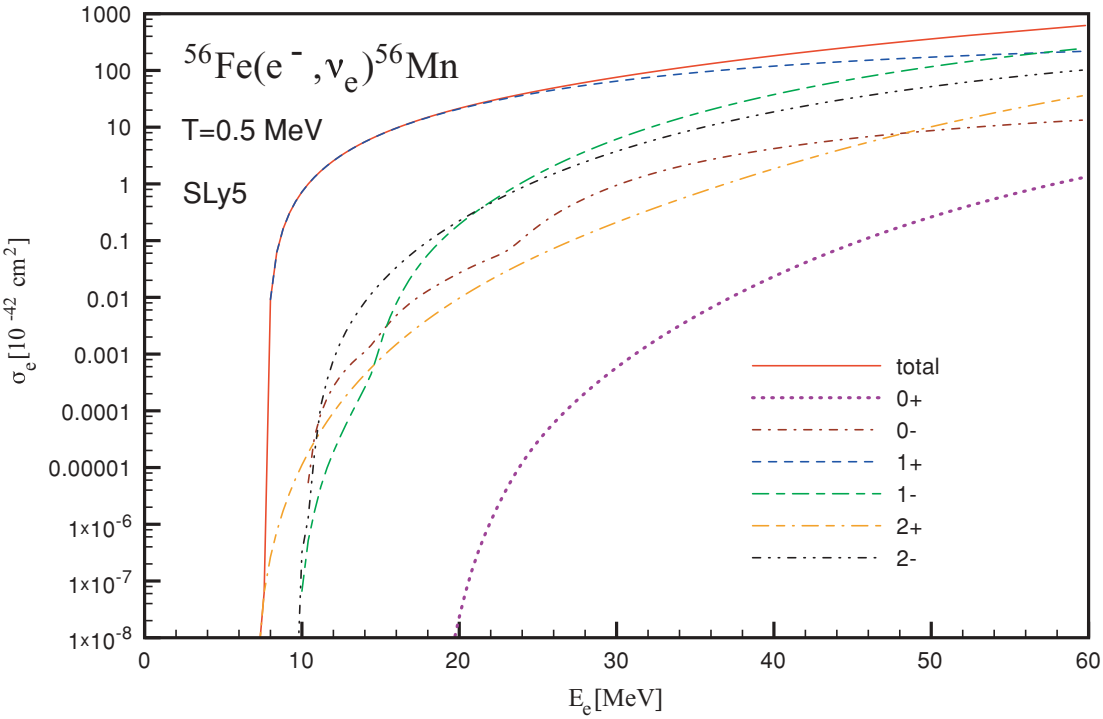

FIG. 7. (Color online) Electron-capture cross section for the ^{56}Fe target nucleus at $T = 0.5$ MeV, calculated with the FTHF + FTRPA using the SLy5 Skyrme effective interaction. In addition to the total cross section, which includes multipole transitions $J^\pi = 0^\pm$, $1^\pm$, and $2^\pm$, contributions from the individual channels are shown in the plot as functions of the incident electron energy E_e.

values predicted by various models in the low-energy interval will not have a pronounced effect on the electron-capture rates [9]. Note, however, that in general this will depend strongly on the matter density and temperature of the environment. More important could be the differences at higher electron energies $E_e > 10$ MeV, for which the Skyrme HF + RPA model systematically predicts cross sections above the values based on the SMMC model. The reason for this systematic effect is most probably that SMMC calculations are carried out only in the $0\hbar\omega$ fp-shell space. Note also that the spread in the calculated cross sections at low energies is greatly reduced for higher incident energies and that above $E_e \approx 15$ MeV all Skyrme effective interactions used in the present HF + RPA calculation effectively predict a universal behavior of the total electron-capture cross sections.

In general, for heavier nuclei and higher electron incident energies, not only the 1^+ but other multipole transitions will also contribute to the total cross section for electron capture [cf. the sums in Eq. (20)]. In calculations for the iron-group nuclei based on the shell model, the cross sections were calculated only from the $0\hbar\omega$ GT strength distributions [6,9]. In Fig. 7 we plot the electron-capture cross section for the ^{56}Fe target nucleus at $T = 0.5$ MeV, calculated with the FTSHF + FTRPA using the SLy5 Skyrme effective interaction. In addition to the total cross section, which includes multipole transitions $J^\pi = 0^\pm$, $1^\pm$, and $2^\pm$, contributions from the individual channels are shown in the plot as functions of the incident electron energy E_e. In this case, the total cross section is completely dominated by the 1^+ channel all the way up to $E_e \approx 30$ MeV, with contributions from other channels being orders of magnitude smaller. Only at very high electron energies do contributions from other multipole transitions become sizable.

Finally, in Fig. 8 we illustrate the isotopic dependence of electron-capture cross sections. Cross sections for even-even Ni target nuclei [i.e., for the reactions ^{A}Ni$(e^-,\nu_e)^A$Co, $A = 56$–62, $T = 0.5$ MeV] are calculated in the FTHF + FTRPA with the Skyrme SLy5 interaction. At any given incident electron energy, the calculated cross sections decrease systematically along the Ni isotope chain because more and more neutron orbitals become occupied and therefore inaccessible for electron-capture reactions. Because with the increase of the number of neutrons the Q value for electron capture increases, more energetic electrons are required for the capture reaction on neutron-rich isotopes and, at any given electron energy, the total cross sections are smaller. We note that the predicted isotopic dependence of electron-capture cross sections in Ni nuclei is in qualitative agreement with the results of the SMMC-based study of Ref. [9].

IV. STELLAR ELECTRON CAPTURE ON NEUTRON-RICH Ge ISOTOPES

At higher densities and temperatures $T \approx 1$ MeV during the collapse phase, electrons are also captured on heavier and more neutron-rich nuclei with protons in the pf shell ($Z < 40$) and neutrons $N \geqslant 40$. In a naive independent-particle picture, the GT transitions, as is shown in Sec. III to dominate electron capture in the pf shell, are forbidden for nuclei with $Z < 40$ and $N \geqslant 40$. However, as has been demonstrated in several

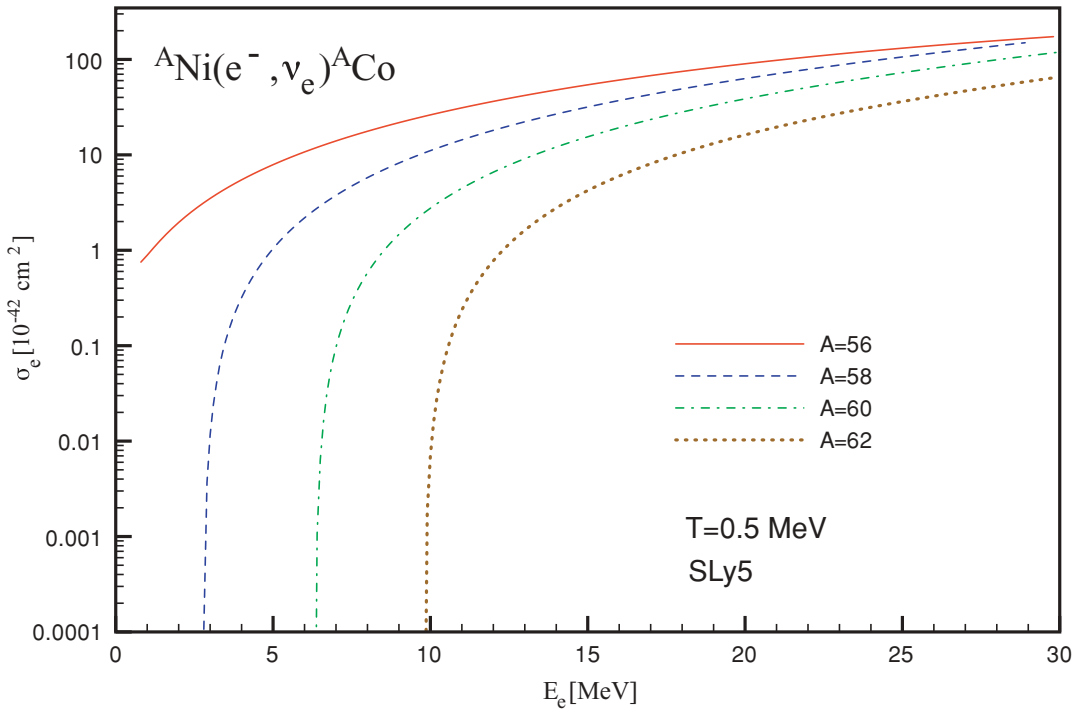

FIG. 8. (Color online) Electron-capture cross sections for the even-even Ni target nuclei ($A = 56$–62) at $T = 0.5$ MeV, calculated with the FTHF + FTRPA using the SLy5 Skyrme effective interaction.

studies, GT transitions in these nuclei are unblocked by finite-temperature excitations. A very detailed study based on the RPA [47] has shown that electron capture on nuclei with protons in the pf shell and $N > 40$ can compete with capture on free protons if forbidden transitions are taken into account in addition to allowed ones. At high temperatures $T \sim 1.5$ MeV, GT transitions are thermally unblocked as a result of the excitation of neutrons from the pf shell into the $g_{9/2}$ orbital. In Ref. [10] a hybrid model has been introduced to calculate electron-capture rates on neutron-rich nuclei in this mass region. In the hybrid model the temperature and configuration-mixing effects are taken into account with the SMMC method and are described by partial occupation numbers for the various single-particle orbits. Using mean-field wave function with finite-temperature occupation numbers determined from SMMC, the electron-capture cross sections are calculated with an RPA approach. Both allowed GT and forbidden transitions are included in the calculation. The SMMC/RPA hybrid approach was applied to the even germanium isotopes $^{68-76}$Ge at typical core-collapse temperatures $T \sim$ 0.5–1.3 MeV, and it was demonstrated that configuration mixing is strong enough to unblock the GT transitions at all temperatures relevant to core-collapse supernovae [10]. The SMMC/RPA model was also used to calculate rates for electron capture on nuclei with mass numbers $A = 65$–112 at temperature and densities characteristic for core collapse [11]. It was shown that electron capture on nuclei dominates over capture on free protons, and simulations of core collapse have demonstrated that these capture rates produce a strong effect on the core collapse trajectory and the properties of the core at bounce.

In the present analysis we apply the self-consistent FTSHF + RPA model in the calculation of stellar electron-capture cross sections on neutron-rich Ge nuclei and compare the results with those obtained by Langanke, Kolbe, and Dean [10] using the hybrid SMMC/RPA model. In Fig. 9 we plot the various Skyrme HF + RPA electron-capture cross sections for the reaction ^{72}Ge(e^-,ν_e)^{72}Ga at $T = 0.5$ MeV as functions of the incident electron energy E_e in comparison with the SMMC/RPA results. As in the calculation for the iron-group nuclei in Sec. III, the set of Skyrme effective interactions includes SGII [33], SkM* [43], SLy4 [44], SLy5 [45], and SkO$'$ [46]. A given interaction is used consistently in both the FTSHF equations that determine the single-nucleon basis and the matrix equations of the FTRPA model. The SMMC calculation of Ref. [10] included the complete ($pfg_{9/2}$) shell-model space and used a pairing + quadrupole residual interaction with parameters adjusted for this mass region. The single-particle energies were adopted from the KB3 interaction, but the $f_{5/2}$ orbital was artificially reduced by 1 MeV to simulate the effects of the $\sigma\tau$ component that is missing in the residual interaction. An energy splitting of 3 MeV between the $g_{9/2}$ and the $f_{5/2}$ orbitals was assumed. For the RPA calculation based on SMMC, the single-particle energies were taken from a Woods-Saxon parametrization, and the residual interaction is a finite-range G matrix derived from the Bonn nucleon-nucleon potential [48]. In the calculation of total cross sections, both models include the multipole transitions $J^\pi = 0^\pm$, $1^\pm$, and $2^\pm$. In the SMMC/RPA calculation, the GT strength is quenched by multiplying the GT transition matrix elements by the constant factor 0.7. In the present analysis, the standard reduction of the axial vector coupling constant

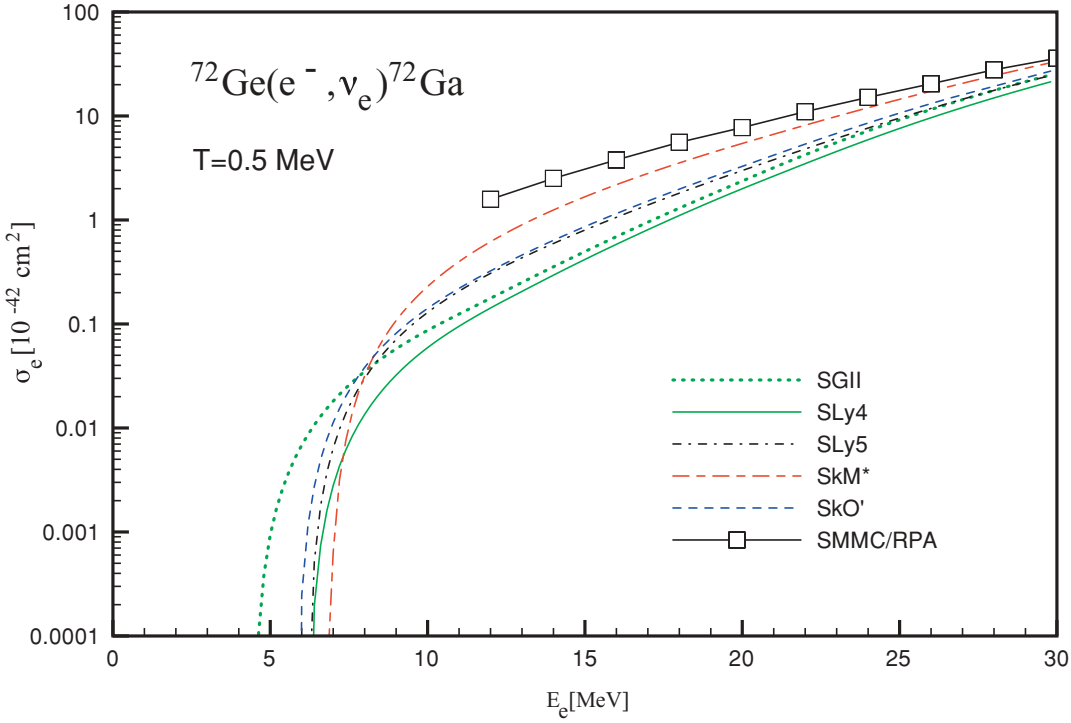

FIG. 9. (Color online) Electron-capture cross sections for the reaction ^{72}Ge(e^-,ν_e)^{72}Ga at $T = 0.5$ MeV as functions of the incident electron energy E_e. The Skyrme HF + RPA results are compared with cross sections calculated with the hybrid SMMC/RPA model [10].

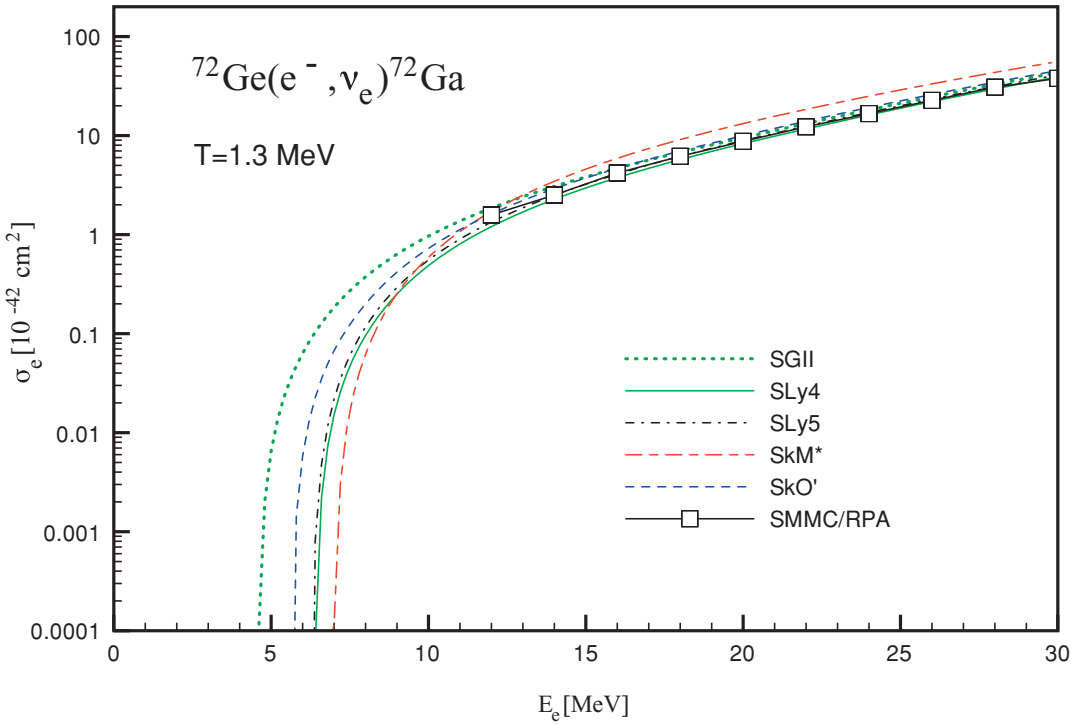

FIG. 10. (Color online) Same as Fig. 9, but for the temperature $T = 1.3$ MeV.

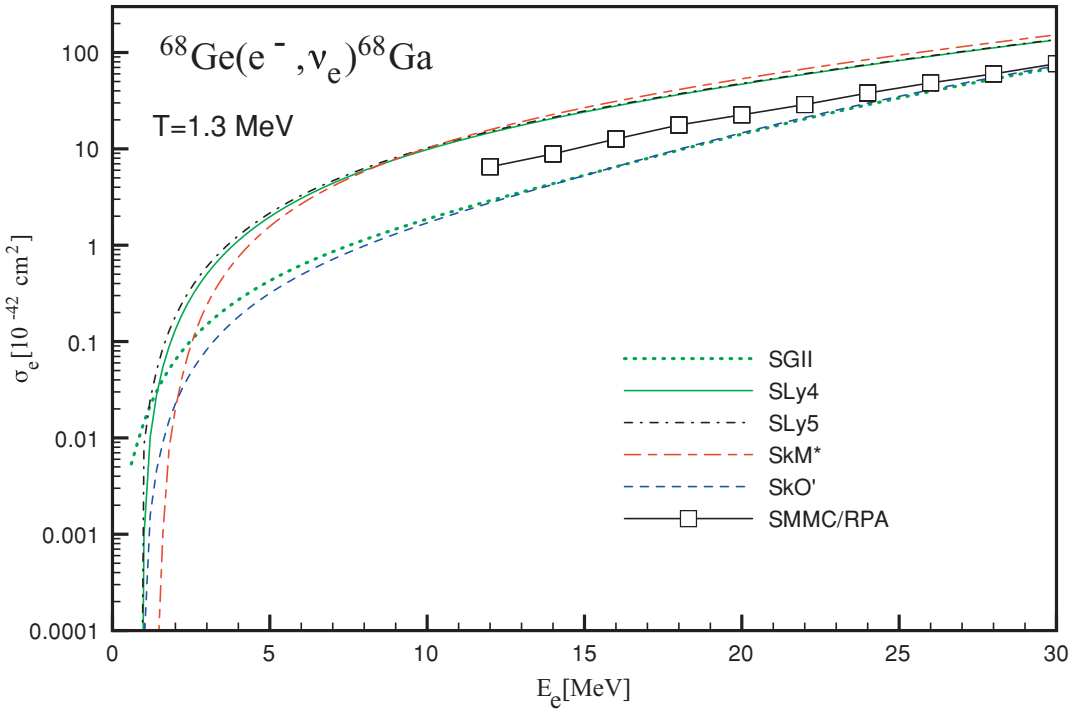

FIG. 11. (Color online) Same as Fig. 9, but for ^{68}Ge at $T = 1.3$ MeV.

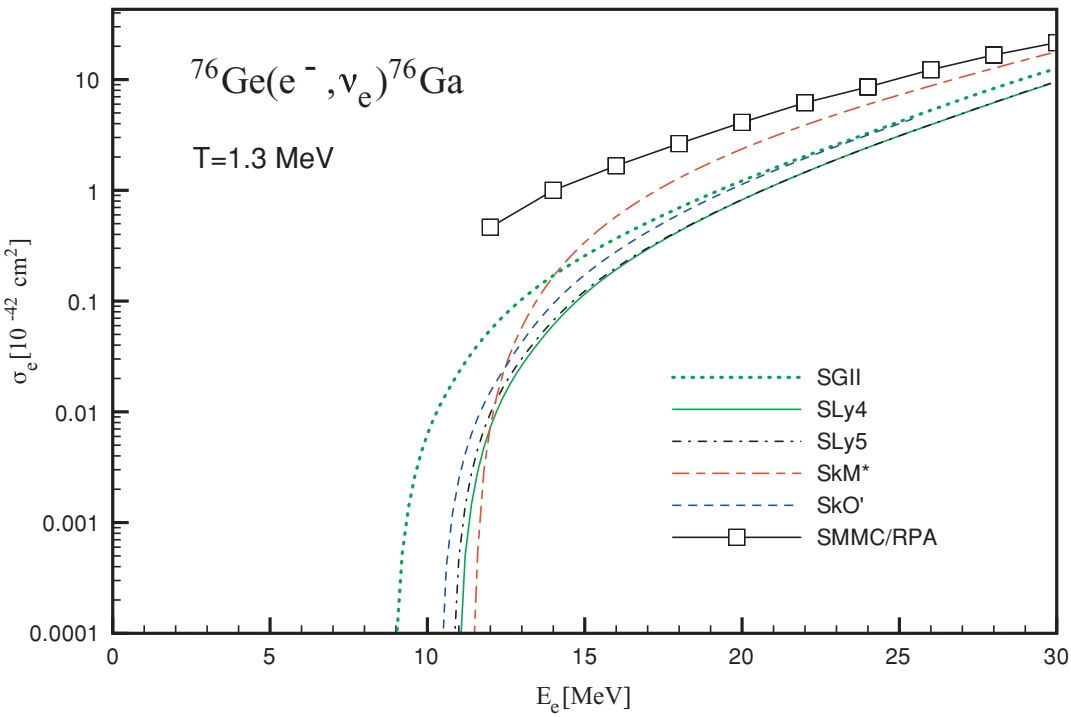

FIG. 12. (Color online) Same as Fig. 9, but for ^{76}Ge at $T = 1.3$ MeV.

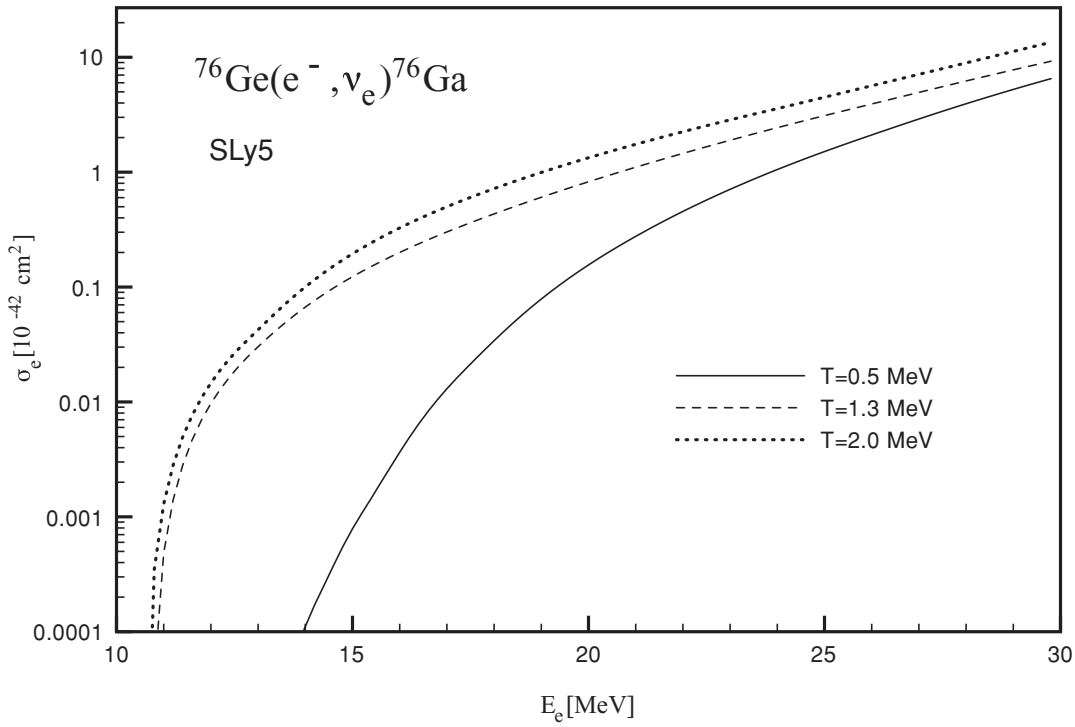

FIG. 13. Electron-capture cross sections for the ^{76}Ge target nucleus at temperatures $T = 0.5$, 1.3, and 2.0 MeV, calculated with the FTSHF + FTRPA using the SLy5 Skyrme effective interaction.

$g_A = 1.262 \rightarrow g_A = 1.0$ is employed, which corresponds to the quenching factor 0.8.

Similar to the case of iron-group nuclei, the cross sections calculated with different Skyrme parametrizations display a spread of values of less than an order of magnitude at lower electron energies. At higher incident energies the differences between values calculated with different effective interactions are much smaller. In general, the FTSHF + FTRPA results are in good agreement with the cross sections calculated in the hybrid SMMC/RPA model, especially at higher electron energies $E_e > 20$ MeV. At lower energies, the SMMC/RPA cross sections are considerably above the results obtained in the present calculation. The FTSHF + FTRPA calculations have also been carried out at higher temperature $T = 1.3$ MeV (Fig. 10). It is interesting to note that in this particular case the FTSHF + FTRPA results are indeed very close to those obtained with the SMMC/RPA model. Note that in Ref. [10] values of the calculated cross sections are reported only for incident electron energies $E_e > 12$ MeV.

In Figs. 11 and 12 the electron-capture cross sections are shown for the ^{68}Ge and ^{76}Ge target nuclei, respectively, at $T = 1.3$ MeV. The FTSHF + FTRPA results are in qualitative agreement with the values calculated using the SMMC/RPA model. For ^{68}Ge, in particular, the Skyrme interactions divide into two branches: SLy4, SLy5, and SkM* predict cross sections that are systematically larger than those obtained from the SMMC/RPA model, whereas cross sections calculated with SGII and SkO′ are below the SMMC/RPA results for electron energies $E_e < 30$ MeV. The FTSHF + FTRPA cross sections are systematically smaller than the values predicted by the hybrid SMMC/RPA model for the target nucleus ^{76}Ge. The isotopic dependence of the electron-capture cross sections, illustrated in Fig. 8 for the even-even Ni nuclei, is also observed in Figs. 10–12 for the Ge isotopes. With the increase of the neutron number the threshold for electron capture is shifted toward higher electron energies, reflecting the change in the Q value. For a given electron incident energy, the total cross section is reduced with the increase in the number of neutrons.

Finally, in Fig. 13 we illustrate the temperature dependence of electron capture on ^{76}Ge. The cross sections are calculated with the FTHF + FTRPA model at three temperatures, $T = 0.5$, 1.3, and 2.0 MeV, using the SLy5 parametrization. The notable increase in the calculated cross sections occurs between $T = 0.5$ MeV and $T = 1.3$ MeV and this corresponds to a significant thermal unblocking of the neutron $p_{3/2}$, $f_{5/2}$, and $p_{1/2}$ orbitals (cf. Figs. 1 and 2 for the case of ^{74}Ge). Because these orbitals are already unblocked at $T = 1.3$ MeV, a further increase in temperature to $T = 2.0$ MeV results in only a moderate enhancement of the electron-capture cross sections.

V. SUMMARY AND CONCLUSIONS

Recent advances in modeling nuclear structure phenomena have also had a strong impact on astrophysical applications. More and more often calculations of stellar nucleosynthesis, nuclear aspects of supernova collapse and explosion, and neutrino-induced reactions are based on microscopic global predictions for the nuclear ingredients rather than on simplified semiempirical approaches. In general, the required nuclear input includes properties of hundreds of nuclei at and far from the line of β stability, including the characteristics

of strong-, electromagnetic-, and weak-interaction processes. Many of these nuclei, especially on the neutron-rich side, are not accessible in experiments; therefore, nuclear astrophysics calculations depend crucially on accurate theoretical predictions for the nuclear masses, bulk properties, nuclear excitations, (n,γ) and (γ,n) rates, α- and β-decay half-lives, fission probabilities, electron and neutrino capture rates, etc.

Improved microscopic stellar weak-interaction rates, evaluated with large-scale shell-model diagonalization and/or hybrid RPA models, have been employed in recent studies of presupernova evolution of massive stars, and it has been shown that the resulting changes in the lepton-to-baryon ratio and iron core mass lead to significant changes in the hydrodynamics of core collapse and the supernova explosion mechanism. These results have emphasized the need for accurate microscopic evaluations of nuclear weak-interaction rates, at densities and temperatures characteristic for core collapse, that can be extended over arbitrary mass regions of the nuclide chart. In this work, for the first time a self-consistent microscopic framework for calculation of weak-interaction rates at finite temperature has been introduced, based on Skyrme functionals. Single-nucleon levels, wave functions, and thermal occupation factors for the initial nuclear state are determined in the FTSHF model, and transitions to excited states are computed using the corresponding FTRPA. Effective interactions are implemented self-consistently, meaning both the finite-temperature single-nucleon HF equations and the matrix equations of RPA are based on the same Skyrme energy density functional.

The model has been employed in illustrative calculations for stellar electron capture on selected nuclei in the iron-group mass region and for neutron-rich isotopes of germanium. Electron-capture cross sections have been calculated as functions of the energy of the incident electron for a representative set of Skyrme functionals. By using different Skyrme functionals one is able to estimate the range of theoretical uncertainty of the HF + RPA approach. For the iron-group nuclei, the results have been compared with those of Ref. [9], where the SMMC model was used to calculate GT^+ strength distributions and electron-capture cross sections and rates were computed in the zero-momentum transfer limit. At low incident electron energies, at which the cross sections are sensitive to the discrete level structure of the GT transitions, all Skyrme HF + RPA cross sections are smaller than the values based on SMMC calculations. These cross sections, however, are very small and the differences among various models will not have a pronounced effect on the calculated electron capture rates. More important could be the differences at higher electron energies $E_e > 10$ MeV, for which the Skyrme HF + RPA model systematically predicts cross sections larger than the values evaluated with the SMMC model. It must be emphasized that the RPA approach takes into account large configuration spaces so that for any multipole operator the whole sum rule is exhausted, whereas generally this is not the case in shell-model calculations.

For electron capture on neutron-rich Ge nuclei, the finite-temperature Skyrme HF + RPA cross sections have been analyzed in comparison with results obtained using the hybrid SMMC/RPA model [10], in which the nucleus is described as a Slater determinant with thermal occupation numbers determined with the SMMC model and capture rates are computed using a charge-exchange RPA built on top of the temperature-dependent Slater determinant. In general, a very good agreement has been found between the FTSHF + FTRPA results and the cross sections calculated using the hybrid SMMC/RPA model, especially at higher electron energies $E_e > 20$ MeV and higher temperatures $T > 1$ MeV. In all cases the two models predict a similar dependence of the cross sections on electron energy in the interval $12 \leqslant E_e \leqslant 30$ MeV. There are, however, differences in the absolute values, especially at relatively low temperature ($T = 0.5$ MeV) and electron energies $E_e < 20$ MeV and for heavier isotopes (e.g., ^{76}Ge).

The results of the present study show that the finite-temperature Skyrme HF plus charge-exchange RPA framework provides a valuable universal tool for the evaluation of stellar weak-interaction rates. Based on a universal Skyrme energy density functional, in the sense that the same functional is used for all nuclei, this framework can be employed in studies of weak-interaction processes in different mass regions. At relevant incident electron energies the absolute spread in the electron-capture cross sections, computed with a variety of Skyrme functionals, is less than an order of magnitude. The next step will be a more extensive calculation and tabulation of electron-capture rates for nuclei in the mass range $A \approx 60$–80, which can be compared with modern semiempirical estimates of weak-interaction rates for intermediate mass nuclei, calculated using available experimental information and simple estimates for the strength distributions and transition matrix elements [49]. For open-shell nuclei at very low temperatures, and especially for calculation of β-decay rates, the framework could be extended to include pairing correlations. In the zero-temperature limit, isobaric analog states and GT resonances in open-shell nuclei have recently been studied with the newly developed self-consistent quasiparticle charge-exchange RPA based on Skyrme functionals [50,51]. Another interesting extension of the model would be the use of a different class of nuclear energy density functionals (EDFs), for instance relativistic EDFs, in which case excited states could be calculated using the charge-exchange relativistic QRPA [52].

ACKNOWLEDGMENTS

This work was supported in part by the Unity Through Knowledge Fund (UKF Grant No. 17/08), the MZOS Project 1191005-1010, and NExEN ANR-07-BLAN-0256-01.

[1] H. A. Bethe, Rev. Mod. Phys. **62**, 801 (1990).
[2] K. Langanke and G. Martínez-Pinedo, Rev. Mod. Phys. **75**, 819 (2003).
[3] H.-Th. Janka, K. Langanke, A. Marek, G. Martínez-Pinedo, and B. Müller, Phys. Rep. **442**, 38 (2007).

[4] H. A. Bethe, G. E. Brown, J. Applegate, and J. M. Lattimer, Nucl. Phys. **A324**, 487 (1979).
[5] G. M. Fuller, W. A. Fowler, and M. J. Newman, Astrophys. J. Suppl. Ser. **42**, 447 (1980); **48**, 279 (1982); Astrophys. J. **252**, 715 (1982); **293**, 1 (1985).
[6] K. Langanke and G. Martínez-Pinedo, Nucl. Phys. **A673**, 481 (2000).
[7] G. Martínez-Pinedo, K. Langanke, and D. J. Dean, Astrophys. J. Suppl. Ser. **126**, 493 (2000).
[8] A. Heger, K. Langanke, G. Martínez-Pinedo, and S. E. Woosley, Phys. Rev. Lett. **86**, 1678 (2001).
[9] D. J. Dean, K. Langanke, L. Chatterjee, P. B. Radha, and M. R. Strayer, Phys. Rev. C **58**, 536 (1998).
[10] K. Langanke, E. Kolbe, and D. J. Dean, Phys. Rev. C **63**, 032801(R) (2001).
[11] K. Langanke *et al.*, Phys. Rev. Lett. **90**, 241102 (2003).
[12] W. R. Hix, O. E. B. Messer, A. Mezzacappa, M. Liebendörfer, J. M. Sampaio, K. Langanke, D. J. Dean, and G. Martínez-Pinedo, Phys. Rev. Lett. **91**, 201102 (2003).
[13] M. Bender, P.-H. Heenen, and P.-G. Reinhard, Rev. Mod. Phys. **75**, 121 (2003).
[14] D. Vretenar, A. V. Afanasjev, G. A. Lalazissis, and P. Ring, Phys. Rep. **409**, 101 (2005).
[15] H. M. Sommermann, Ann. Phys. (NY) **151**, 163 (1983).
[16] E. Khan, N. Van Giai, and M. Grasso, Nucl. Phys. **A731**, 311 (2004).
[17] E. Khan, N. Van Giai, and N. Sandulescu, Nucl. Phys. **A789**, 94 (2007).
[18] A. L. Goodman, Nucl. Phys. **A352**, 30 (1981).
[19] A. L. Goodman, Nucl. Phys. **A352**, 45 (1981).
[20] P. Bonche, S. Levit, and D. Vautherin, Nucl. Phys. **A427**, 278 (1984).
[21] J. des Cloizeaux, in *Many-Body Physics, Les Houches, 1967*, edited by C. De Witt and R. Balian (Gordon and Breach, New York, 1968).
[22] D. Vautherin and N. Vinh Mau, Nucl. Phys. **A422**, 140 (1984).
[23] W. Besold, P.-G. Reinhard, and C. Toepffer, Nucl. Phys. **A431**, 1 (1984).
[24] H. Sagawa and G. F. Bertsch, Phys. Lett. **B146**, 138 (1984).
[25] P. F. Bortignon, R. A. Broglia, G. F. Bertch, and J. Pacheco, Nucl. Phys. **A460**, 149 (1986).
[26] F. Alasia and O. Civitarese, Phys. Rev. C **42**, 1335 (1990).
[27] Ph. Chomaz, D. Vautherin, and N. Vinh Mau, Phys. Lett. **B242**, 313 (1990).
[28] O. Civitarese and M. Reboiro, Phys. Rev. C **63**, 034323 (2001).
[29] J. L. Egido and P. Ring, J. Phys. G: Nucl. Part. Phys. **19**, 1 (1993).
[30] D. Lacroix, P. Chomaz, and S. Ayik, Phys. Rev. C **58**, 2154 (1998).
[31] A. N. Storozhenko, A. I. Vdovin, A. Ventura, and A. I. Blokhin, Phys. Rev. C **69**, 064320 (2004).
[32] P. Ring and P. Schuck, *The Nuclear Many-Body Problem* (Springer, Heidelberg-Berlin, 1980).
[33] N. Van Giai and H. Sagawa, Nucl. Phys. **A371**, 1 (1981).
[34] K. Ikeda, S. Fujii, and J. I. Fujita, Phys. Lett. **3**, 271 (1963).
[35] J. S. O'Connell, T. W. Donnely, and J. D. Walecka, Phys. Rev. C **6**, 719 (1972).
[36] J. D. Walecka, in *Muon Physics*, edited by V. M. Hughes and C. S. Wu (Academic Press, New York, 1975), pp. 113–218.
[37] J. D. Walecka, *Theoretical Nuclear and Subnuclear Physics* (Imperial College Press and World Scientific, London, 2004).
[38] E. Kolbe, K. Langanke, G. Martínez-Pinedo, and P. Vogel, J. Phys. G **29**, 2569 (2003).
[39] T. Kuramoto, M. Fukugita, Y. Kohyama, and K. Kubodera, Nucl. Phys. **A512**, 711 (1990).
[40] G. Audi, A. H. Wapstra, and C. Thibault, Nucl. Phys. **A729**, 337 (2003).
[41] M. B. Aufderheide, I. Fushiki, S. E. Woosley, and D. H. Hartmann, Astrophys. J. Suppl. Ser. **91**, 389 (1994).
[42] A. Poves and A. Zuker, Phys. Rep. **70**, 235 (1981).
[43] J. Bartel, P. Quentin, M. Brack, C. Guet, and H.-B. Hakansson, Nucl. Phys. **A386**, 79 (1982).
[44] E. Chabanat, P. Bonche, P. Haensel, J. Meyer, and R. Schaeffer, Nucl. Phys. **A627**, 710 (1997).
[45] E. Chabanat, P. Bonche, P. Haensel, J. Meyer, and R. Schaeffer, Nucl. Phys. **A635**, 231 (1998).
[46] P.-G. Reinhard, D. J. Dean, W. Nazarewicz, J. Dobaczewski, J. A. Maruhn, and M. R. Strayer, Phys. Rev. C **60**, 014316 (1999).
[47] J. Cooperstein and J. Wambach, Nucl. Phys. **A420**, 591 (1984).
[48] E. Kolbe, K. Langanke, and P. Vogel, Nucl. Phys. **A652**, 91 (1999).
[49] J. Pruet and G. M. Fuller, Astrophys. J. Suppl. Ser. **149**, 189 (2003).
[50] S. Fracasso and G. Colò, Phys. Rev. C **72**, 064310 (2005).
[51] S. Fracasso and G. Colò, Phys. Rev. C **76**, 044307 (2007).
[52] N. Paar, T. Nikšić, D. Vretenar, and P. Ring, Phys. Rev. C **69**, 054303 (2004).